






Underwater surveys reveal deep-sea corals in newly explored regions of the southwest Atlantic

Nayara F. Carvalho ^{1✉}, Linda G. Waters¹, Renata C. M. Arantes², Daniel M. Couto¹, Guarani H. Cavalcanti³, Arthur Z. Güth ¹, Ana Paula C. Falcão⁴, Paula D. Nagata¹, Cízia M. Hercos³, Dalton K. Sasaki ¹, Marcelo Dottori¹, Erik E. Cordes ⁵ & Paulo Y. G. Sumida ^{1✉}

Deep-sea coral distribution and composition are unknown in much of the global ocean, but repurposing ocean industry surveys can fill that gap. In Santos Basin, southeast Brazil, areas (241–963 m depth) were surveyed during seven Petrobras cruises, mapping bottom topography with multibeam sonar, then collecting video with remotely operated vehicles. Here, we defined deep-sea coral species distribution and richness, using these surveys, correlating them to physical oceanographic properties. *Solenosmilia variabilis* was the most prevalent colonial species in coral mounds. Overall, 67% of species were Octocorallia. Coral assemblage structure, abundance, and richness varied among sites both within and among depths, with higher density and richness in the northernmost Santos basin. Depth was the strongest predictor for scleractinian coral distribution, with depth ranges varying by species. Assemblage differences corresponded to changes in water mass. *Desmophyllum pertusum* was more abundant in South Atlantic Central Water and *S. variabilis* in Antarctic Intermediate Water influenced areas.

¹Instituto Oceanográfico, Universidade de São Paulo, São Paulo, SP, Brazil. ²Programa de Pós-graduação em Oceanografia, Universidade Federal de Santa Catarina, Florianópolis, SC, Brazil. ³Centro de Pesquisa, Desenvolvimento e Inovação Leopoldo A. Miguez de Mello - Petrobras, Rio de Janeiro, RJ, Brazil. ⁴Gerência de geodésia e Oceanografia da Petrobras, Rio de Janeiro, RJ, Brazil. ⁵Department of Biology, Temple University, Philadelphia, PA, USA.
✉email: nayarafc@usp.br; psumida@usp.br

The geographic extent of deep-sea corals (DSC) is far from being fully understood¹. Throughout the world's oceans, elucidation of the processes that determine their spatial patterns and abundances will improve our understanding of the structure of continental margin communities. At each new location explored, many new DSC species have been revealed and notable differences in the distribution and habitat preferences of different coral taxa observed^{2–4}.

With advancements in the use of technology in offshore areas, considerable progress in DSC research has occurred⁵. Ecological surveys typically state the depth range of recorded species and the most and least frequent and/or abundant taxa found. Data on species composition and abundances may give insight into many aspects of the community, including population dynamics and ecological interactions like competition and predation⁶. The establishment of these DSC sites requires specific physical, chemical, and geological conditions, including parameters such as temperature, salinity, dissolved oxygen concentration, current intensity, and substratum^{7–9}. Depth ranges vary for each species depending on regional variables, such as water mass structure and bathymetric gradients in productivity^{10,11}. Thus, understanding the requirements for establishing DSC habitats and the variability in depth ranges among species, we can gain a comprehensive understanding of the dynamics and interactions within the studied communities.

Model outputs have indicated that continental slopes are one of the main suitable coral sites worldwide⁸. The bathyal (~200–3000 m depth) region¹² has large protruding topographical features, interfering with bottom current flow and creating colonizable hard substrates at multiple depths; this enhances seabed erosion and resuspends particulates, which provides an elevated supply of suspended food particles for corals¹³. Along the Brazilian margin, five main water masses with distinct intensity and transport directions influence the continental slope¹⁴, which may contribute to regional species diversity pools.

Species distribution models presented by ref. ¹⁵ indicated that Santos basin in the Southeastern Brazilian Margin is a suitable region for the presence of DSC. Video recorded by remotely operated vehicles (ROV) during Petrobras surveys in this region detected an abundance of corals. Analyzing these video recordings in the northern region of Santos Basin, this study found that most of the coral sites were coral mounds that were distributed on the middle slope, while coral reef sites dominated the upper slope. The richness of DSC species was characterized, and we examined the following hypotheses that; (1) Vertical distance among samples at two depth strata (upper and middle slope) affects coral communities (species richness and assemblage structure) on a local scale, more than geographic horizontal distance (three different areas at the same depth); and (2) spatial distribution patterns of DSC species occur as a function of environmental factors (physicochemical properties). Although some species have broad distributions, most species occurred more frequently on the middle slope; richness was high in areas D and E (at the same depth). The possible influence of physical water properties on DSC richness and assemblage structure was then examined, finding a relation between assemblages and water mass differences.

Results

Water mass characteristics. The historical collection of CTD data in the vicinity of areas A–E recorded an average temperature of 14.40; 9.56; 4.25; 4.41 and 4.60 °C, respectively (Fig. 1). In 50 years, the highest temperature range was approximately four degrees and occurred around area A, with a minimum

temperature of 12.38 and maximum of 16.61 °C. Area B presented temperatures ranging between 7.99 and 11.07 °C, and areas C, D and E showed almost no variability over the years (3.79–4.74; 4–4.78; 4.13–4.99 °C, respectively).

Salinity historical records in the vicinity of areas A–E recorded an average of 35.58; 34.93; 34.51; 34.49 and 34.50, respectively (Fig. 1). Salinity did not vary notably around each sampled area among years, with a maximum observed range of 0.63 (Area A). The lowest and highest salinity values recorded for each area were: 35.27–35.90, area A; 34.70–35.12, area B; 34.40–34.64, area C; 34.45–34.54, area D; and 34.40–34.53, area E. Because historical data were studied around each sampled area, the temperature and salinity profiles are grouped according to their spatial position (Fig. 1).

The T–S diagrams indicated the presence of two main water masses influencing the sampling areas: SACW with neutral densities between 26.35 and 27.10 kg m⁻³; AAIW between 27.10 and 27.60 kg m⁻³; (Fig. 2). Temperature and salinity values associated with area A are majorly within the density range of SACW, while values associated with area B lie in a transition density range (~27.10 kg m⁻³) between SACW and AAIW. In the deepest levels (areas C, D and E), the dominant water mass is the AAIW.

Coral sites. The 69 studied deep-sea coral sites comprise three distinct morphological features: living coral reefs, live coral reefs on the top of deep-sea coral carbonate mounds, and extinct coral carbonate mounds where the framework building corals are no longer alive and growing.

Considering their biological and geological characteristics, the upper slope coral formations (area A) are reef sites. Colonies of *D. pertusum* (formerly *Lophelia pertusa*) composed of living polyps at their extremities and a large volume of dead coral structure underneath (a volume that exceeds the living portion), characterize dense reef sites around 245 m deep, with few associated DSC (Fig. 3). This is the beginning of coral mound formation, but there has not been sufficient time for coral skeleton to accumulate to the extent where it shrouds the underlying substrata.

At a depth of 494 m on the upper slope, area B was identified as a coral carbonate mound. Although we could not extract cores from the specific mounds examined in this study to verify whether they contain many years of alternation of coral skeletons with sediment, every coral formation exhibiting the surface characteristics described in ref. ¹¹ was considered a deep-sea coral carbonate mound.

In area B, the studied coral carbonate mound was found in association with live *D. pertusum* forming reef structures, with several associated DSC (Fig. 3). In contrast, no live *D. pertusum* forming reef structures were observed at the studied sites on the middle slope. At greater depths, which correspond to the reflective targets studied between 785 and 963 m, the coral formations on the middle slope (areas C, D, and E) consisted of extinct coral carbonate mounds that were colonized by solitary scleractinian corals, individual colonies of scleractinian corals, octocorals, and black corals (Antipatharia).

Deep-sea coral assemblage characterization. The species accumulation curves indicated a more comprehensive sampling effort when all coral sites in the northern Santos Basin were combined (Supplementary Fig. 1). The species accumulation curves for the upper slope did not reach an asymptote, suggesting that additional coral species could be found with increased sampling effort, whereas the sampling effort in the middle slope was relatively sufficient (Supplementary Fig. 1). Regarding the study areas, although site A recorded lower richness of DSC, the sampling

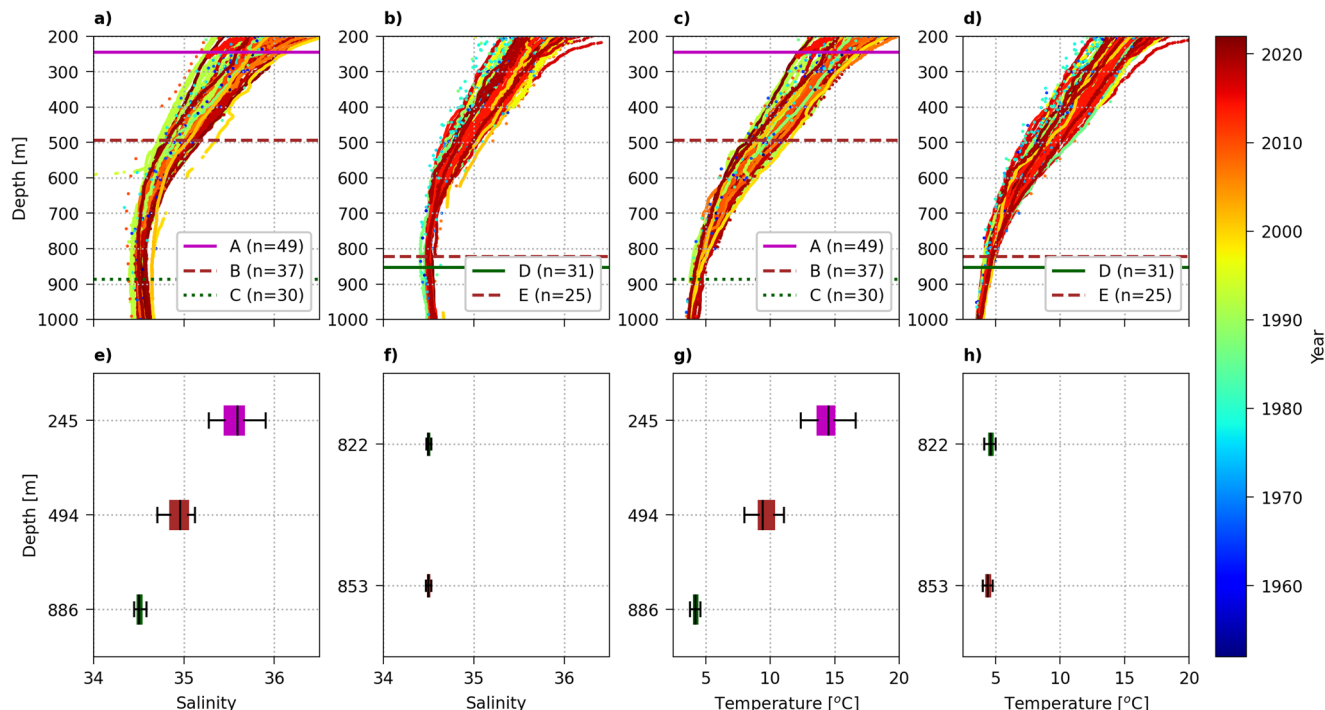


Fig. 1 Profiles of salinity and temperature. Historical (a, b) practical salinity and (c, d) potential temperature profiles within a radius of ~20 km of positions A, B, C, D, E. Positions A, B, C, D, E depths are 245, 494, 886, 822, and 853 m, respectively. The number of CTD casts with valid data within the site bottom depth (horizontal colored lines) ± 5 m are indicated by 'n'. Boxplots of (e, f) salinity and (g, h) temperature were calculated by selecting valid data within the above-mentioned radius and vertical interval range. In the boxplots, the central value represents the median value, the box represent quartiles, while the whiskers show the quartile $\pm 1.5 \times$ interquartile range. The values of the horizontal axes of the top panels correspond to the ranges in the bottom panels.

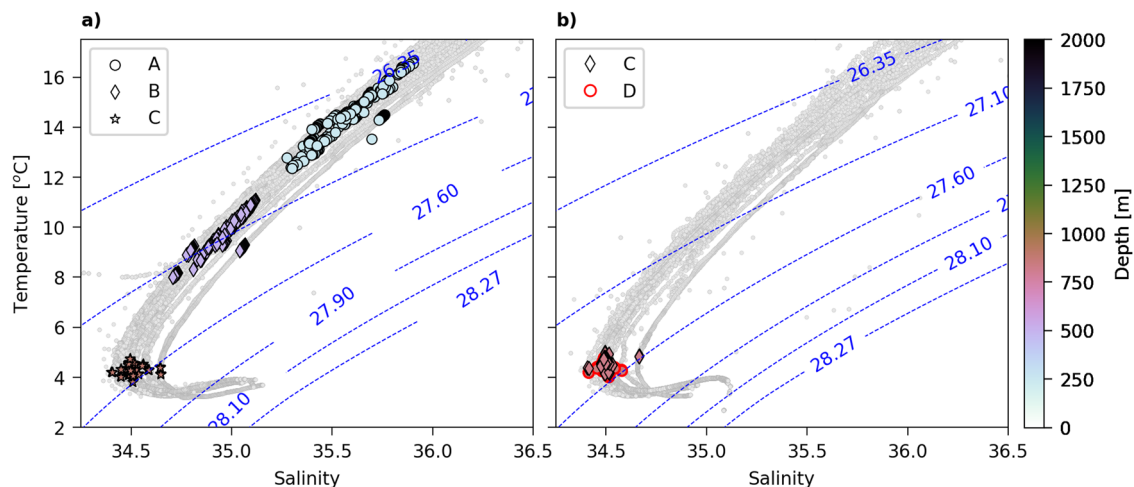


Fig. 2 T-S diagram of historical temperature and salinity. T-S diagram of historical temperature (in situ) and salinity (practical salinity scale) data within a radius of approximately 20 km around individual coral areas (a) A, B, C, (b) D and E. The blue dotted contours depict the neutral density and serve as water mass density limits in the southwestern South Atlantic⁵¹. Colored markers indicate the selected T-S pairs within the vertical range that includes a depth range of the bottom depth ± 5 m. Gray dots represent pairs at other depths. Panel (b) shows the E points superimposed over the D points, as both areas were sampled at similar depths and within similar density ranges.

effort was adequate to produce a representative collection of DSC from the study sites, even though the curve did not reach the asymptote (Supplementary Fig. 1). As for location B, even though there was only one sampling unit (indicating a need for increased sampling effort), it is noteworthy that the survey time, distance covered by the ROV, and the number of frames analyzed in area B revealed an extensive coral site in that region and provided important background information on the deep-sea coral richness recorded (Supplementary Table 1).

A total of 2054 live DSC belonging to 63 taxa were recorded across 69 coral sites (Supplementary Fig. 2). Live scleractinians were the most frequently observed taxa, followed by the Octocorallia group, representing 98% and 90% occurrence, respectively, at the studied coral sites. Antipatharians and Anthoathecata were the least frequently observed taxa (found at 47% and 42% of coral sites, respectively).

The highest richness values were recorded for the taxa Octocorallia, Antipatharia, Scleractinia, and Anthoathecata, in

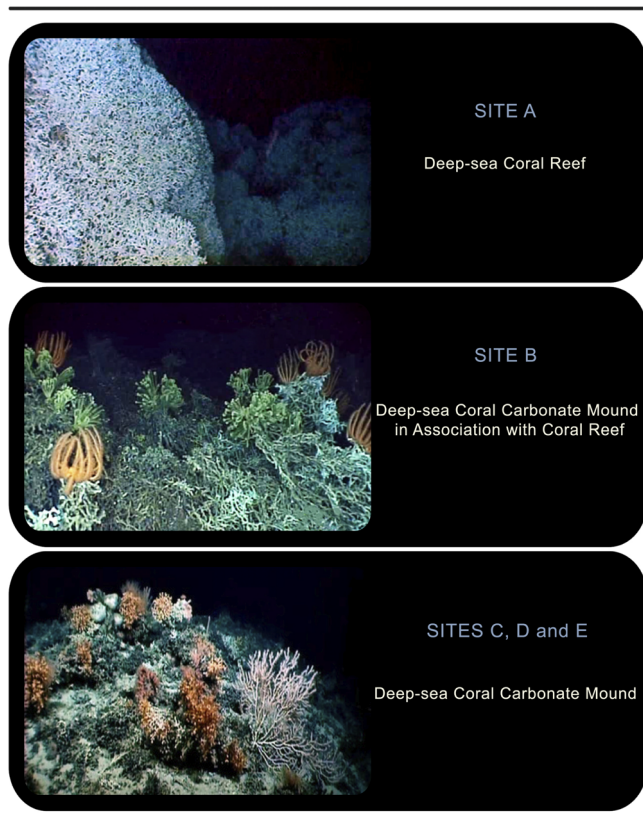


Fig. 3 Coral sites. Three distinct morphological features of coral sites in the study areas. Area A - living coral reefs; Area B - live coral reefs on top of extinct deep-sea coral carbonate mounds; and areas C, D, and E - extinct coral carbonate mounds.

that order. A total of 42 taxa belonging to eight families of Octocorallia were recorded. Although Octocorallia were found in all areas of the study site, among the most common taxa, the species *Paramuricea* sp. 1, *Narella* sp. 1, *Pseudoanthomastus* sp. 1, *Trachythela rudis* sp. 1, and *Keratoisididae* sp. 3 were more frequent in areas C, D, and E, and absent in A (Supplementary Data 1). Notably, two Octocorallia taxa, *Narella* sp. 1 and *Paragorgia* sp. 2, appear to be new to science (publication intended shortly).

Regarding scleractinia, three families (Caryophylliidae, Dendrophylliidae, and Oculinidae) and seven taxa were recorded (Supplementary Data 1). Among them, *Solenosmilia variabilis* and *Desmophyllum pertusum* were the most frequent, representing 85% and 51%, respectively. However, *D. pertusum* was more common in areas A and B, while *S. variabilis* occurred exclusively in areas C, D, and E (Supplementary Data 1). Eleven antipatharians from the Leiopathidae and Schizopathidae families were found, with *Bathypathes* sp. 1 being the most frequent (33%) among black corals. Lastly, the Anthoathecata order had the lowest taxonomic richness, with *Stylasteridae* sp. 1 (35%) being the most frequent (Supplementary Data 1).

In terms of distribution range, the majority of DSC (60%) were limited to the middle slope (785–963 m depth), whereas only 7.3% of the species occurred exclusively on the upper slope (241–502 m depth) (Supplementary Data 1). Among the groups, most Octocorallian species were exclusively found on the mid-slope (30 species or 71%). Scleractinian species had a broad distribution along upper and middle slope regions (4 species or 57%), except for *S. variabilis* and *Enallopsammia rostrata*, which were restricted to the middle slope, and *Pourtalesmilia* sp. 1 on

the upper slope (Supplementary Data 1). Antipatharians were also well-represented across all depth strata, while Anthoathecata species were more restricted to the deeper regions (middle slope) (Supplementary Data 1).

Spatial distribution

Vertical distribution - upper and middle slope. Deep-sea coral assemblage frequency (PERMANOVA: Pseudo-F = 64.419, DF = 1, $p = 0.001$) and richness (PERMANOVA: Pseudo-F = 7.345, DF = 1, $p = 0.008$) showed significant differences between assemblages on the upper slope (241–494 m) and middle slope (827–939 m depth strata) (Supplementary Table 2).

The DSC frequency SOM training resulted in twenty-five cells arranged in a 6×4 rectangular grid (quantization error = 0.01; topographic error = 0.08). Two distinct assemblage groups were identified, indicating strong gradients in the depth distribution (Fig. 4a, b). The deep coral reef assemblage found on the upper slope, between 241 and 494 m depth, could be clearly distinguished in the cells on the right side of the neural map (cluster 2, gray) (Fig. 4a, b). The second group (cluster 1, light gray) is mainly composed of the assembly registered on the middle slope, between 800 and 1000 m, represented by cells on the left side of the neural map (Fig. 4a, b).

According to BMU (Best Matching Units), among species of DSC that had the highest correlations with the vertical spatial distribution, *D. pertusum*, *P. conferta*, *Leiopathes* sp. 1 and *Madrepora oculata* had high occurrences on the upper slope (cluster 2; gray) (Fig. 4b, c). *S. variabilis*, *Pseudoanthomastus* sp. 1, *Narella* sp. 1, *Keratoisididae* sp. 7, *Victogorgia* sp. 1, *Primnoidea* sp. 2 and *Enallopsammia rostrata* were the main taxa accounting for similarities among middle slope assemblages (cluster 1; light gray) (Fig. 4a, b, c).

The Mantel tests indicated that geographical distances between deep-sea coral sites (areas A, B and C - stratified profile) were not correlated with the DSC assemblage frequency ($r = -0.079$, $P = 0.885$) and richness ($r = -0.146$, $P = 0.958$).

Horizontal distribution. Assemblage (PERMANOVA: Pseudo-F = 5.518, DF = 2, $p < 0.001$), richness (PERMANOVA: Pseudo-F = 23.526, DF = 2, $p < 0.001$), and density (PERMANOVA: Pseudo-F = 18.426, DF = 2, $p < 0.001$) of DSC differed significantly at area C (Fig. 5a). The average richness and density were significantly higher at areas D and E, and lowest in C (Fig. 5a). Octocorallia and Scleractinia also had significantly higher richness and density at areas D and E (Fig. 5a and Supplementary Table 3).

The DSC abundance SOM training resulted in forty cells arranged in a 6×6 rectangular grid (quantization error = 0.01; topographic error = 0.2) and pointed to two distinct groups, indicating different DSC assemblages between coral sites (Fig. 5b, c). Assemblage structure at area C at the bottom of the spatial map (cluster 1; light gray) clearly differed from areas D and E, at the middle and top of the map (cluster 2; gray) (Fig. 5b, c).

Of the species with the highest correlations with the horizontal spatial distribution pattern, according to the BMU (Best Matching Units), *S. variabilis*, *Paramuricea* sp. 1, *Narella* sp. 1, *Desmophyllum* sp. 1, *Trachythela rudis*, *Stolonifera* sp. 1 and *Errina gracilis*, occurred almost exclusively in areas D and E, with their maximum abundance at the middle and upper of the map (cluster 2; gray) (Fig. 5d). In contrast, taxa such as *D. pertusum*, *Pseudoanthomastus* sp. 1, *Keratoisididae* sp. 3 and *Keratoisid* sp. 7 occur throughout the studied area (Fig. 5d), while *Primnoidea* 1 has a higher abundance in area C, seen on the bottom side of the map (cluster 1; light gray) (Fig. 5d).

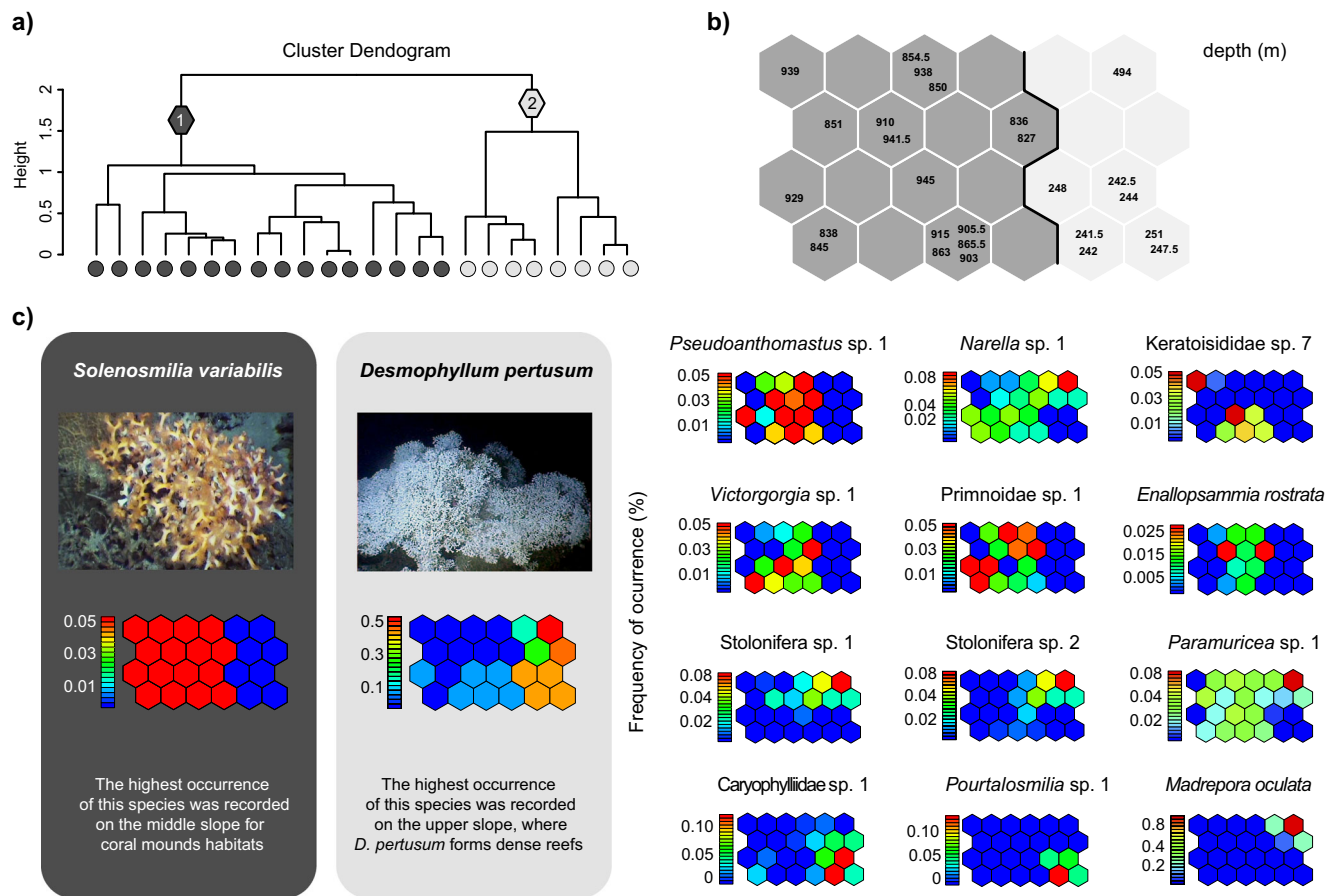


Fig. 4 Vertical distributions - Areas A, B and C. **a** Hierarchical clustering of the trained self-organizing map (SOM) by the Depth; **(b)** Distribution of sampling depths on the SOM, with grayscale zones corresponding to the indicators in the cluster diagram, and **(c)** Distribution patterns of the best match units taxa in the trained SOM according to the frequency of occurrence of DSC. Each map corresponds to one taxa; these can be superimposed onto the map representing the cluster distribution of depths to show at which depths they are more frequently observed.

The mantel test indicated that geographical distances between coral sites (ares C, D and E) were not correlated with the DSC assemblage density (individuals m^{-1}) ($r = 0.004$, $P = 0.577$) and richness ($r = 0.085$, $P = 0.052$).

Relationship between environmental variables and coral assemblages. The principal coordinates analysis (PCO) indicated the relative importance of water masses (physical-chemical environmental parameters) to the distribution and abundance of taxa, with axis 1 explaining 23% and axis 2 explaining 13% of the total variance. The taxa *D. pertusum*, *Caryophylliidae* sp. 1, *Pourtalesmilia* sp. 1 and *Madrepora oculata* were more associated with SACW (Fig. 6). In contrast, most DSC taxa (*Desmophyllum* sp. 1, *Paramuricea* sp. 1, *Narella* sp. 1, *Trachytella rudis*, Keratoisididae sp. 7, *Solenosmilia variabilis*, *Pseudoanthomastus* sp. 1, *Stolonifera* sp. 1 and *Enallopsammia rostrata*) were correlated with AAIW (Fig. 6).

GAM models indicated that temperature and salinity were significant predictors of DSC richness, explaining approximately 30% of the variation (Table 1). Results indicated that DSC taxa showed an optimal range of occurrence from 4 to 6 °C, and salinity values between 34.4 and 34.6 (Fig. 7).

Discussion

This study unveiled previously undescribed deep-sea coral sites and taxonomic richness in the northern Santos Basin, Brazil, at depths ranging from 241 to 963 m and latitudes between

approximately 23 °S and 24 °S. Dense deep-sea coral reef sites were observed on the upper slope coral sites under the influence of the South Atlantic Central Water (SACW), while the carbonate coral mounds sites were found predominantly on the middle slope under the influence of the Antarctic Intermediate Water (AAIW). The vertical and horizontal geographic distances between deep coral sites (measured as linear distance) showed no correlation with the assemblage structure and richness. However, even for the sites located at the same local scale, coral assemblage structure and richness varied according to depth and also among coral carbonate mounds at similar depths.

Despite individual colonies of the framework-forming *Desmophyllum pertusum* occurring in all sampled areas and at 51% of the total studied coral sites, this species only built dense reef-like structures on the upper slope under influence of SACW. It is known that seawater temperature can determine the distribution of DSC¹⁶, taking into account the possibility of local species adaptation¹⁷. While populations in the temperate North Atlantic are known to be affected by temperatures above 15 °C¹⁸, in the tropical South Atlantic, *D. pertusum* has developed under a temperature variation of 12.38 to 16.61 °C, based on the last 50 years of available environmental data.

Considering that the dense *D. pertusum* reef structures on the upper slope of Santos Basin developed within their natural thermal range¹⁷, and taking into account variation in pre-existing metabolic stores or underlying genetic variation¹⁹, the growth of these colonies was likely primarily controlled by food availability. This can be determined by a combination of surface productivity

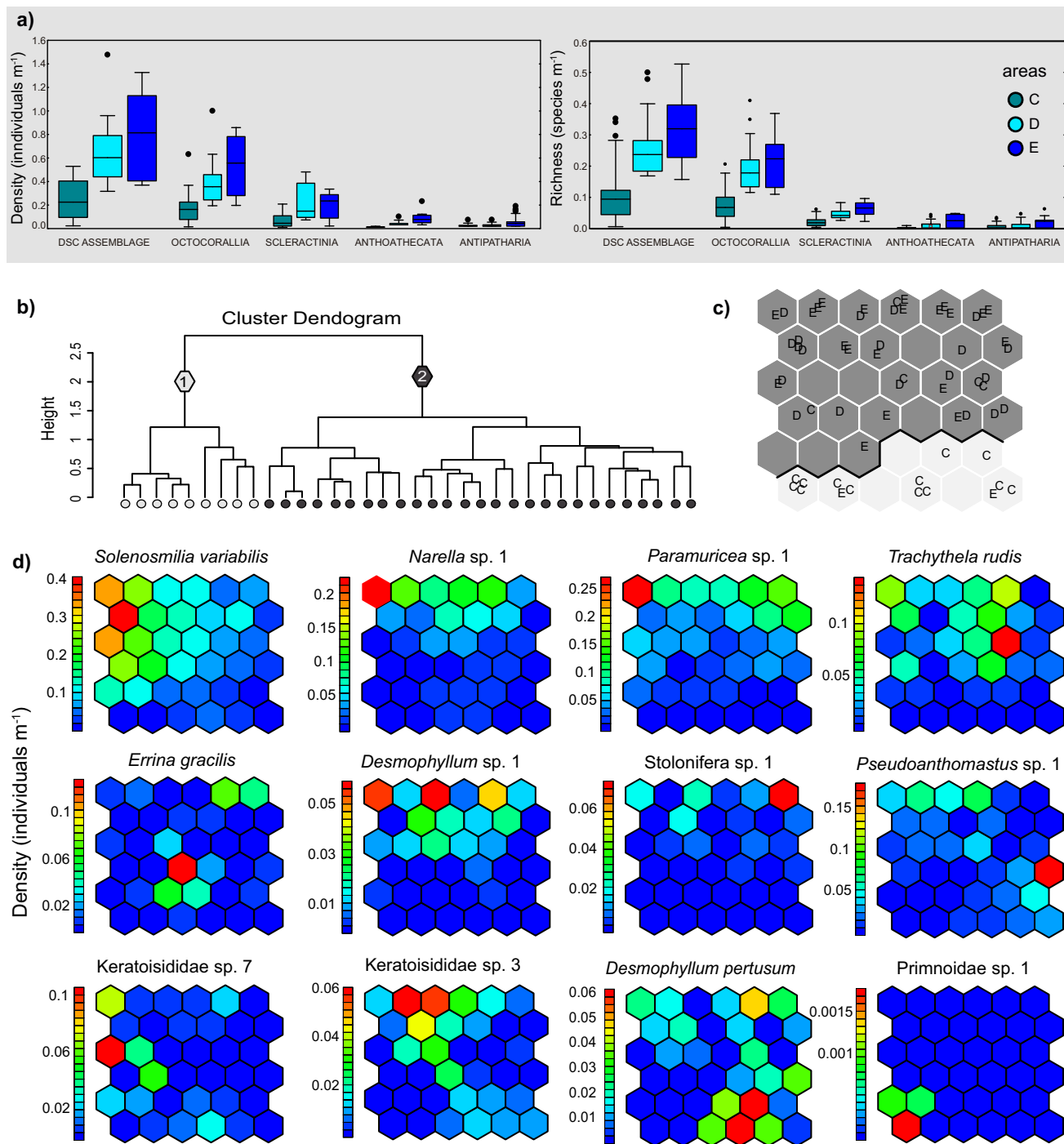


Fig. 5 Horizontal distribution - Areas C, D and E. **a** Individuals m^{-1} and richness of deep-sea corals, Octocorallia, Scleractinia, Antipatharia, and Anthoathecata respectively at each coral site. The boxes show the 25–75% quartile, while circles indicate outliers and whiskers non-outliers. The central line represents the median and rectangular the mean; **(b)** Hierarchical clustering of the trained self-organizing map (SOM) by the coral sites; **(c)** Distribution of sampling coral sites on the SOM, with grayscale zones corresponding to the indicators in the cluster diagram; and **(d)** Distribution patterns of taxa in the trained SOM according to the DSC density. Each map corresponds to one taxa; these can be superimposed onto the map representing the cluster distribution of coral sites, showing at which area they are more frequently observed.

and hydrodynamic processes²⁰ that can complement food sources around this area. Examples of active hydrodynamic processes in the region are the poleward-flowing Brazil Current, and the equatorward Intermediate Western Boundary Current, which respectively influence the top 500 m of the water column, and depths below 500 m²¹.

It is known that reef habitats are the beginning of coral mound formation²². The studied upper slope coral site registered at

494 m depth is a coral carbonate mound with *D. pertusum* colonies building a relatively large reef-like structure on the top (Fig. 4). Nevertheless, the main *D. pertusum* colonial growth forms (morphotypes) in area B look like columnar structures, differing from the “bush-shaped” colonies in area A²³. It suggests a stronger influence of bottom current velocities and water mass characteristics, since this particular site is registered in a transition density range between SACW and AAIW. The columnar

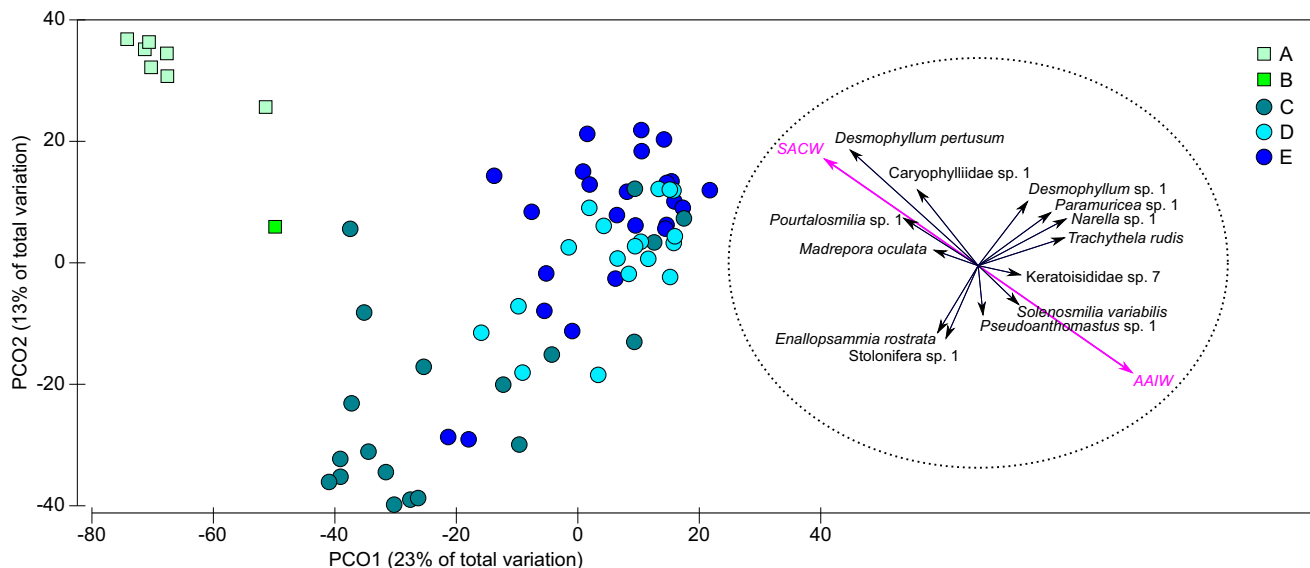


Fig. 6 PCO plots of deep-sea coral taxa and water mass associations. Principal coordinates analysis (PCO) plots based on deep-sea coral taxa (Spearman correlation coefficient ($|r_{SP}| \geq 0.2$) and its association with South Atlantic Central Water (SACW) and Antarctic Intermediate Water (AAIW). Labels: \square Upper slope; \circ Middle slope.

Table 1 Results of the GAM fitted model for deep-sea coral richness and environmental variables.

Deep-sea Coral Richness

| Variables | AIC | SS | Pseudo-F | p | res.df | r ² | # Var. |
|----------------------------------|--------|--------|----------|-------|--------|----------------|--------|
| Temperature | 525.78 | 39356 | 19.864 | 0.001 | 67 | 0.228 | 1 |
| Temperature + Salinity | 525.76 | 7510.7 | 3.958 | 0.001 | 66 | 0.272 | 2 |
| Temperature + Salinity + Density | 523.60 | 3874.7 | 2.075 | 0.062 | 65 | 0.295 | 3 |

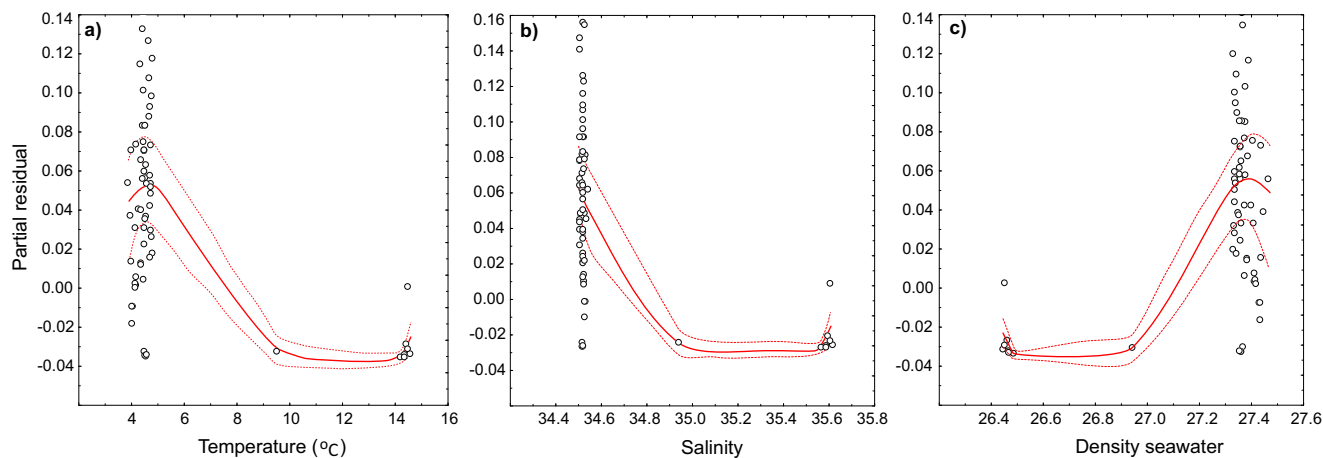


Fig. 7 Relationships between deep-sea corals and environmental variables. GAM analysis illustrating significant relationships of deep-sea coral richness and (a) temperature (°C), (b) salinity and (c) density seawater. Lines represent the estimates of the best models; dashed lines are confidence intervals (95%); circles indicate data sampling points.

architecture represent a growth strategy in response to low flow speeds and/or low food concentrations²³, as opposed to bushy forms, that represent a growth strategy in response to a high energy local environment²³.

Water masses have diverse environmental characteristics, such as distinctive currents, temperature, salinity, nutrients and pH. As depth changes, distinct hydrodynamic regimes and sedimentary processes act on sites^{24,25}. On the middle slope, the framework-forming *Solenosmilia variabilis* was the main live colonial taxa on

the surface of the coral carbonate mounds, with no records for upper slope sites. This species is widely distributed along the Brazilian coast²⁶. The nearest reports that also had a high frequency of occurrence of *S. variabilis* are from the adjacent Campos Basin, with the majority of records between 700 and 1200 m depth¹¹.

S. variabilis are recorded under a temperature variation of 3.79–4.99 °C and salinity variation of 34.49–35.52, corroborating the temperature and salinity in other records and in global

predictive models^{8,27}. Depth, salinity and particulate organic carbon (POC) were the main factors predicting the distribution of *S. variabilis* off the Brazilian margin¹⁵.

The characteristics of AAIW correspond to the zone with the highest taxonomic richness in the present study. Octocorallia is the group responsible for the highest taxonomic richness in the region, accounting for approximately 66% of the registered taxa ($n = 42$). This is not unexpected, as they are known to harbor the highest diversity among coral taxa, with over 3000 described species worldwide²⁸. Thirty-two percent of the Octocorallia taxa had records from a coral site under SACW influence, at $\sim 9.56^\circ\text{C}$ (Area B). However, most of this group is registered on the middle slope, at $\sim 4\text{--}5^\circ\text{C}$.

Although the studied deeper coral sites are under the influence of the same water mass (AAIW), DSC assemblages, abundance, and richness varied among these areas, with a significant increase from C to E. Species such as *S. variabilis*, *Paramuricea* sp. 1, *Narella* sp. 1, *Desmophyllum* sp. 1, *Trachythela rudis*, *Stolonifera* sp. 1 and *Errina gracilis*, occurred almost exclusively in areas D and E. At the northern end of the basin, areas D and E are the closest sites to two physical mechanisms that occur along Cabo Frio, quasi-seasonal coastal upwelling and eddy-induced upwelling^{29,30}. The penetration and surfacing of SACW in the inner shelf region influence ocean productivity³⁰, where mass and energy are transferred through trophic webs³¹. High abundances of marine snow are commonly observed in benthic systems of the Cabo Frio upwelling region³². Thus, high food availability may explain the highest deep-sea coral richness and abundance in the vicinity.

Although upwelling phenomena are important in the structuring of biological communities, further studies will help elucidate some of these deep-sea coral pattern differences among coral carbonate mounds. The lack of correlation found in the mantel test with geographic distance may be due to the analyzed areas being on the same spatial scale (local scale). Thus, distances are not sufficient to cause differences in the assemblages. The coral mounds located in area C are linked to features identified as “pockmarks”³³, which can modify the characteristics of the sediment³⁴, change the current flow³⁵, and harbor diverse and highly specialized fauna^{36,37}. However, it was observed that the richness of DSC is lower in area C, as illustrated in Fig. 7. Therefore, additional investigations are necessary, including the determination of the age/time of formation of the extinct carbonate mounds, the presence of erosive grooves associated with the action of bottom currents, and other relevant features.

The Brazilian slope was identified as a favorable region for deep-sea coral habitats¹⁵, and the number of recorded taxa in the SW Atlantic has been increasing in recently explored areas^{11,24–26,34,38–41}. However, access to deep-sea science data in unexplored regions is extremely limited, primarily due to high costs⁴². Therefore, industry-science partnerships have provided valuable databases to enhance and expedite scientific discovery in these areas^{43,44}.

The southeastern slope of Brazil has accumulated a substantial amount of environmental and biological data, collected using a diverse array of underwater technologies by the PETROBRAS company. This deep-sea coral study conducted with an ROV in the Santos Basin, which identified morphospecies, is expected to improve the assessment of deep-sea coral richness in the area. ROV data is an underutilized scientific resource with substantial intrinsic value and global coverage⁴², and its benefits outweigh potential limitations associated with industry-provided data analysis.

Despite the concentration of ROV exploration efforts in areas of industry interest and the lack of standardized methodology in offshore operations, which may compromise the analysis of

qualitative and quantitative data, the provided database has enabled the present study and is crucial for establishing basic knowledge about DSC in Brazil. DSC taxonomy is complex, and morphological descriptions sometimes lack sufficient clarity, which could result in biodiversity underestimation. Video footage resolution may also limit DSC identification. The image quality obtained from an ROV, particularly older models, can sometimes preclude accurate species-level identification⁴⁵. Therefore, it is likely that the known inventory will grow with increased sampling effort as well as with the use of molecular tools, essential for assisting classical taxonomy⁴⁶.

Deep coral-reef systems are clearly complex, where a number of overlapping ecological and physical processes may simultaneously influence DSC assemblage structure. The results of the present work make an important contribution to understanding the distribution and ecology of DSC on the continental slope. DSC distribution and composition were defined in previously unexplored regions in the northern Santos basin in the Southwestern Atlantic. The most frequently occurring stony coral was *Solenosmilia variabilis*. *D. pertusum* primarily inhabited areas with the presence of SACW whereas *S. variabilis* occurred predominantly at depths with the presence of AAIW. The differences in DSC abundance and richness occurred among studied sites with the influence of the temperature and salinity. However, as with all models that seek to explain the structure of assemblages, a substantial proportion of the variation was not explained, indicating the influence of other factors. Here, we propose that water mass may be an important predictor for determining DSC distribution patterns of the most dominant reef-forming species.

Methods

Study area. The study region, Santos Basin off the coast of Brazil, is located in the southwest (SW) Atlantic Ocean, with an area $\sim 350,000\text{ km}^2$ ⁴⁷. Data were collected from the upper (241–251 m depth, area A; 494 m depth, area B) and middle slope (827–945 m depth, area C; 815–963 m depth, area D; 785–876 m, area E;) in the northern Santos Basin (Fig. 1), where the isobaths are narrow and the shelf break occurs between 120 and 180 m depth⁴⁸.

A regional bathymetric map derived from a mosaic of single beam echosounder data from the Brazilian Navy, nautical charts, depth data from the Brazilian Continental Shelf Survey Plan, 3D seismic data (especially of the continental slope and São Paulo Plateau) and multibeam surveys, which was provided by PCR-BS (Projeto de Caracterização Regional da Bacia de Santos)⁴⁹, illustrates that the study areas are on the upper and middle slope, between 241 and 963 m depth (Fig. 8). A slope gradient map derived from a bathymetric grid highlights the seafloor morphology around the studied areas. The areas are located on a smooth slope, with gradients varying from 0.65 to 2° (Fig. 8).

The water column in the studied region (up to 1000 m depth) is composed of three water masses: Tropical Water (TW; 0–150 m), South Atlantic Central Water (SACW; 150–500 m) and Antarctic Intermediate Water (AAIW; 500–1000 m)^{14,50}. TW is oligotrophic, warm ($>20^\circ\text{C}$) and saline (>36)^{14,50}, within which phytoplankton blooms occur that supply food to the seafloor. Below the TW is the SACW, pycnocline water formed by subsidence at the Subtropical Convergence⁵⁰, with temperatures varying from 6 to 18°C and salinities from 34.6 to 36, tending to dominate the mid to outer-shelf. Underneath it, the AAIW is characterized by a water column salinity minimum and being oxygen-rich^{5,14}.

Water mass characteristics. To identify the water properties (such as temperature and salinity) and its variability around the deep coralline studied areas, a collection of CTD casts over the continental shelf and slope was used. It consists of measurements made by historical oceanographic surveys and argo floats, spanning from November 1972 to March 2022. Selected hydrographic databases were obtained from NOAA’s National Oceanographic Data Center, the Brazilian Navy, Argo program and from Instituto Oceanográfico at the University of São Paulo. The collection and organization are part of efforts of the PCR-BS Project (Santos Basin Environmental Characterization). All casts were binned to a vertical grid with a 1 m resolution.

Water mass identification was based on neutral density ranges (Supplementary Table 4) identified by ref. ⁵¹. Neutral density⁵² was computed using the original ‘gamma-n’ fortran package (v3.1) wrapped in python. The practical salinity scale and in situ temperature were used to calculate neutral density.

Data collection. Prior to ROV imaging, data from seafloor geophysical surveys previously carried out by Petrobras were analyzed to increase the chances of

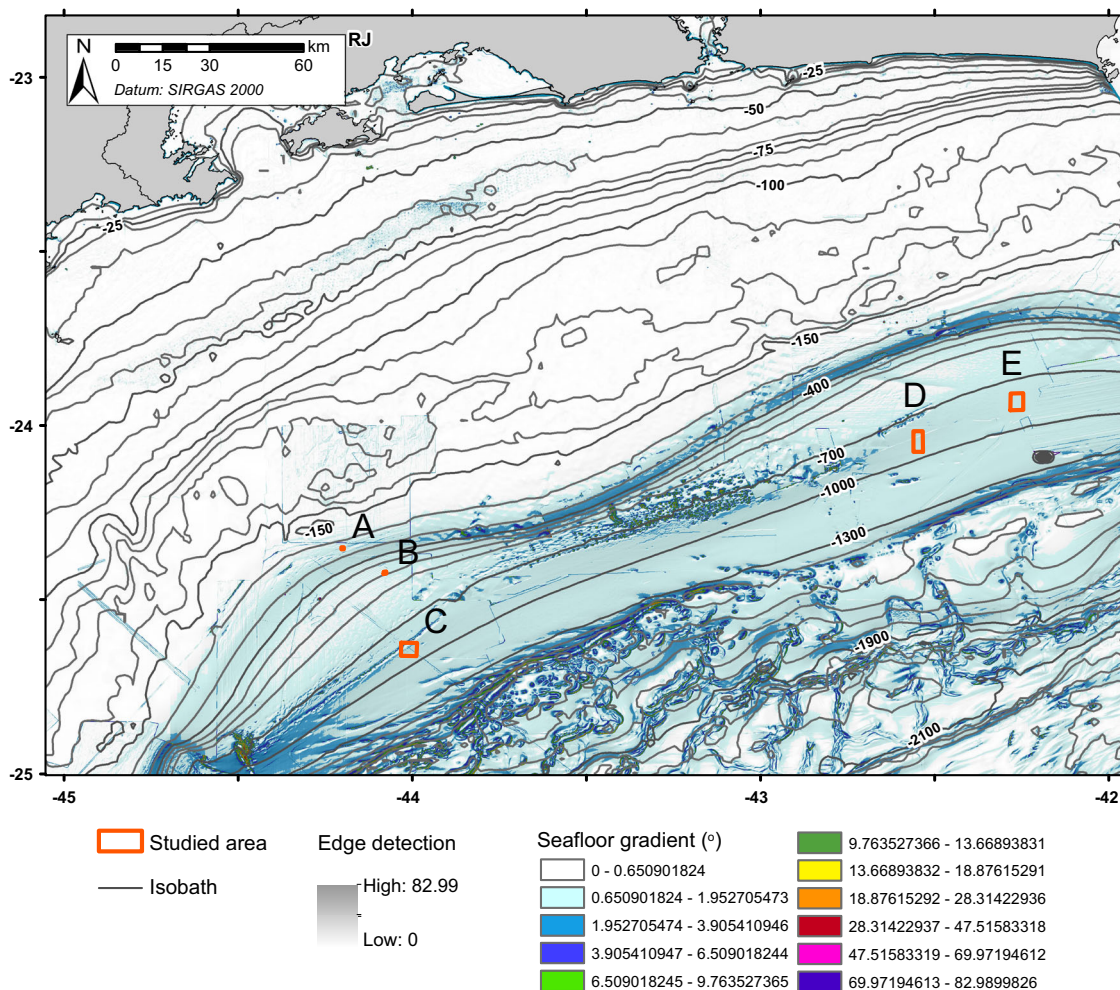


Fig. 8 Study area map. Map of the study areas (A; B; C; D; E) showing the location of the northern Santos Basin in southeastern Brazil; SW Atlantic.

finding DSC sites (the same approach was applied in the adjacent Basin, see ref. 11). These data were collected using a multibeam echosounder, indicating a large number of acoustically strongly-reflective targets between 200 and 1000 m depth. These targets typically correspond to hard substrata, thus indicating sites of interest for further exploration by ROV¹¹.

Selecting some sites with strongly-reflective targets (identified as coral sites), a deep-sea coral image database was generated using ROV videos from five areas, during seven research cruises (Fig.8). Videos were recorded within the study sites between 2009 and 2012, resulting in approximately 179 h of video at depths ranging from 241 to 963 m (Supplementary Table 1).

The videos were collected by ROV survey ships contracted by Petrobras through the SENSIMAR Project (Sensitive Marine Environments of Southeast Brazil) to perform environmental surveys as well as routine oil and gas industry inspections. They were equipped with multiple video cameras that varied in resolution. Laser scales were not used and high definition video was available only in more recent operations. The ROV traversed slowly, close to the bottom. Occasionally the ROV paths were interrupted for sampling and detailed camera zooms. Images were obtained from the continuously recorded video for each coral site.

Image data processing and analysis. Prior to image analysis, one still “JPG” frame was generated for every five seconds of video recording using ffmpeg software (version 4.2.2) at each coral site, and each live coral colony in the field of view was identified from its closest-range images. Close range images facilitated species recognition by allowing clear visualization of small colonies or other coral species. Low-quality images (e.g., unfocused, with high turbidity, or low illumination, among others) were discarded.

Because identification to the lowest taxonomic level was not always possible through images, distinguishing morphological characteristics were used to assign putative species or “morphospecies”⁵³. Species level identification was performed according to gross morphology, branching pattern, polyp size, and type^{53–58}.

Data pre-treatment. Camera arrangement, camera type, and logging methods differed between surveys. Therefore, to test the null hypothesis that DSC assemblage composition did not differ among years, an Analysis of Similarity (ANOSIM) was carried out using PRIMER v6 with the PERMANOVA + software package. Since no difference was found (Global $R = 0.061$, $p = 0.417$), the different years were grouped into a single data set for further analyses. This improved the power of the tests related to the study of spatial distribution.

Deep-sea corals assemblage characterization. The sampling effort was evaluated using a species accumulation curve, with a non-parametric bootstrap⁵⁹, for three different situations: a) the studied coral sites in the Santos Basin, b) the studied coral sites on the upper slope (areas A and B) and middle slope (areas C, D, and E); and c) coral sites located in each studied area (A, B, C, D, and E). This method assumes that all species occur randomly, without taking species abundance into account. The index estimates were obtained through the analytical equation of ref. 60 using the EstimateS software⁶¹.

Deep-sea coral assemblages were characterized by the frequency of occurrence (FO), which represents the percentage of each taxon’s occurrence compared to the total number of coral sites analyzed in each of the areas A, B, C, D, and E (Supplementary Table 1). Abundance, on the other hand, refers to the actual number of individuals of a specific species present in a given area or community. In this study, density of live DSC, which is the abundance per meter of track, was calculated solely for coral sites in areas C, D and E. Richness and density estimates were based on DSC from the coral site ROV video record in relation to the total track of each site (individuals/richness per meter of track). Species richness was recorded for each coral site in each area: A, B, C, D, and E.

Spatial distributions. A permutational multivariate analysis of variance (PERMANOVA)⁶² was performed twice, examining both vertical and horizontal distribution of the coral species. When overall significant differences were detected, pairwise tests with Bonferroni correction for multiple tests (sites C, D and E) were performed using the ‘pairwise.adonis’ function in the R Package ‘pairwiseAdonis’⁶³.

An unsupervised machine learning technique, a self-organizing map (SOM) training algorithm^{64,65}, was then used to characterize DSC assemblage patterns for several depths (vertical distribution) and areas (horizontal distribution). The SOM was generated using the software “An Interactive Machine Learning App for Environmental Science”, an open-source application available on GitHub⁶⁶.

The SOM was formed by two layers of artificial neurons, the input layer (nodes or neurons that are computational units) and the output layer (neurons arranged in a two-dimensional grid), both connected through weights⁶⁵. In SOM analysis, each sample is treated as an n -dimensional input vector defined by its variables⁶⁷. The input vector is fed by the input layer into a neural network and each is connected to an output vector with a single weight vector⁶⁸. The SOM output is an ordered two-dimensional map composed of nodes called neurons; each is connected to its neighbors by a neighborhood relationship that dictates the map's structure.

The basic SOM training algorithm consists of three phases. In the first phase (competitive), the output neuron that presents the weight vector with the smallest distance from the input is considered the winner, also called BMU (Best Matching Unit). In the second phase (cooperative) the neighborhood of this neuron is defined. Finally, the last phase (adaptive) occurs when the weights of the code vectors of the winning neuron and its neighborhood are adjusted, making it possible to detect similarities between the samples.

In the present work, each sample was assigned to an output neuron that has a coefficient vector associated with the input data. The coefficient vector is referred to as a weight vector W between the input and output layers. The weights establish a connection between the input units (deep-sea coral species) and their associated output units (coral sites).

The algorithm can be described as follows: when an input vector x is presented to the SOM, in this case, frequency occurrence data of DSC species (first SOM testing depth differences) and the density (ind m^{-1}) of each DSC species (second SOM testing spatial differences), the neurons in the output layer compete with each other, and the winner (whose weight is the minimum distance from the input vector) is chosen. The winner and its predefined neighbors in the algorithm update their weight vectors according to the SOM learning rules as follows:

$$m_{ij}(t+1) = w_{ij} + \alpha(t) \cdot h_{jc}(t) [x_i(t) - m_{ij}(t)]$$

where $m_{ij}(t)$ represents the weight between a node i in the input layer and a node j in the output layer at iteration time t . The learning rate factor $\alpha(t)$ is a decreasing function of iteration time t . The neighborhood function $h_{jc}(t)$ is a smoothing kernel defined over the points of the lattice that determines the size of the neighborhood of the winning node (c) to be updated during the learning process. This learning process continues until all the weight vectors have completed their interactions.

In the present work, as neighborhood functions between neurons were tested in the bubble function and the iterative training process, we chose to use 500 iterations. After training, the WardD2 linkage method was applied to a hierarchical cluster analysis (HCA) to highlight sets of real objects on the map⁶⁹. The “elbow method (or knee method)” was used to determine the ideal number of clusters⁷⁰. Therefore, the final map will show similar data samples close to each other (groups) and dissimilar data samples far from each other. As error quantification criteria, the average quantization error (QE) and the topological error (TE) are calculated. The average quantization error is the average distance between each data vector and its ‘best matching unit’ (BMU), measuring the resolution of the map. For the Kohonen map grid, the topological error indicates the accuracy of mapping in terms of preserving the topology⁶⁵.

A Mantel test (Pearson's correlation) with 5000 permutations⁷¹, was used to test the hypothesis that assemblage structure and richness of DSC are correlated to vertical and horizontal geographic distances between DSC sites (linear distance - meters). The analyses were performed in the R statistical environment (The R Development Core Team, 2009) using functions from the vegan package⁷².

Vertical distribution - upper and middle slope: In the statistical analyses of vertical distributions, areas A, B and C were used to assess the differences between coral community assemblages at different depths, eliminating areas D and E to reduce possible interference from additional factors in more geographically distant areas. In addition, to avoid underestimation errors, species frequency data was used (instead of density data - $\text{individuals.m}^{-1}$), because areas A and B contain dense reefs of *Desmophyllum pertusum* (formerly *Lophelia pertusa*) that made it impossible to count live coral colonies, obscuring the density determination.

In the first PERMANOVA analysis, the depth data were divided into upper slope and middle slope to facilitate sampling design analysis and the visualization of DSC variation along the vertical gradient. Thus, two depth strata (241–494 m - upper slope, and 827–945 m - middle slope) were the prediction factors for the DSC assemblage frequency occurrence ($\log_{10}(x+1)$ transformed data - Jaccard similarity matrices) and species richness ($\log_{10}(x+1)$ transformed data - Euclidean distance matrices).

In the first training process, the SOM used an input layer comprising 47 nodes (one by taxa) connected to the sampling datasets of 2 depth strata. Prior to analysis, the species frequency was $\log_{10}(x+1)$ transformed for the SOM training run. The subsequent learning phase determined the ‘best matching unit’ based on the Euclidean distance measure. Further ordering and tuning phases were repeated to adjust the neighboring units.

In the Mantel test, to evaluate the effects of geographic distances at vertical strata in the DSC structure, we used two biological matrices. The first was the DSC assemblage frequency (Jaccard similarity measure) and the second was based on the richness of DSC (Euclidean similarity measure). The spatial matrix was the linear geographic distance (distance similarity measure) between the centroid of areas A, B and C.

Horizontal distribution - middle slope: In the second PERMANOVA analysis, we tested the hypothesis that the DSC assemblages varied with areas. Areas C, D, and E (all coral mound sites within the same depth strata) were used as predictors for assemblage structure. The dependent variables were DSC group and assemblage ($\log_{10}(x+1)$ transformed density data - Bray Curtis similarity matrices), species richness, and density of live DSC per meter of each studied coral mound ($\log_{10}(x+1)$ transformed data - Euclidean distance matrices). To avoid underestimation errors, coral abundance data from areas A and B were removed from this particular analysis as these areas contained dense *D. pertusum* reefs that obscured determination of density (see Fig. 3).

The second training process for the SOM used an input layer including 55 nodes (one by taxa) connected to the sampling datasets from three areas. Prior to analysis, the species density data were $\log_{10}(x+1)$ transformed for the SOM training run. The subsequent learning phase determined the ‘best matching unit’ based on the Bray-Curtis index.

To evaluate the effects of geographic distances at horizontal distribution of the DSC structure, we used two biological matrices. The first was the DSC assemblage density (Bray-Curtis similarity measure) and the second a richness of DSC (Euclidean similarity measure). The spatial matrix was a linear geographic distance (distance similarity measure) between the centroid of areas C, D and E.

Relationship between environmental variables and coral assemblages. To summarize multivariate patterns in DSC assemblages across different temperatures, salinities and density of seawater, PCO was performed. Displayed species showed a Spearman correlation coefficient ($|r_{SP}| \geq 0.2$ with one or more axes. All multivariate analyses were performed using PRIMER v6 with the PERMANOVA + software package. Generalized additive models (GAM) were used to evaluate the influence of environmental variables on DSC richness, due to the expectancy of the non-linear response of species and predictor variables⁷⁵. A GAM with a Gamma distribution and the log-link function was used for the modeling. The Gamma distribution was chosen after exploring several alternative distributions (e.g., Gaussian, Poisson, and negative binomial). This distribution is appropriate for continuous, positive, and asymmetric data. Model selection was performed using Akaike information criterion (AIC). The relative importance of each predictor and complete model were evaluated by the R2 statistic.

Reporting summary. Further information on research design is available in the Nature Portfolio Reporting Summary linked to this article.

Data availability

All data generated or analyzed during this study are included in this published article and its supplementary data 1, which is available from Figshare (<https://doi.org/10.6084/m9.figshare.23620962>), as well as the supplementary information files. Any additional data supporting the findings of this study are available upon request to the corresponding authors (nayaraf@usp.br, psumida@usp.br).

Code availability

The code used to analyze these data and generate the results presented in the study can be obtained from <https://github.com/DaniloCVieira/iMESc>.

Received: 15 May 2022; Accepted: 7 July 2023;

Published online: 08 August 2023

References

- Vertino, A., Stolarski, J., Bosellini, F. R. & Taviani, M. Mediterranean corals through time: from Miocene to present. In *The Mediterranean Sea: Its history and present challenges* (eds. Goffredo, S. & Dubinsky, Z.) 257–274 (Springer, 2014).
- Gass, S. E. & Willison, J. H. An assessment of the distribution of deep-sea corals in Atlantic Canada by using both scientific and local forms of knowledge. In *Cold-water Corals and Ecosystems* (eds. Freiwald, A. & Roberts, J. M.) 223–245 (Springer, 2005).
- Watling, L. & Auster, P. J. Distribution of deep-water Alcyonacea off the Northeast coast of the United States. In *Cold-water Corals and Ecosystems* (eds. Freiwald, A. & Roberts, J. M.) 279–296 (Springer, 2005).

4. Auscavitch, S. R. et al. Oceanographic drivers of deep-sea coral species distribution and community assembly on seamounts, islands, atolls, and reefs within the Phoenix Islands protected area. *Front. Mar. Sci.* **7**, 42 (2020).
5. Henry, L. A. & Roberts, J. M. Global biodiversity in cold-water coral reef ecosystems. In *Marine animal forests: the ecology of benthic biodiversity hotspots* (eds. Rossi, S., Bramanti, L., Gori, A. & Orejas, C.). 235–256 (Springer, 2017).
6. Verberk, W. C. E. P. Explaining general patterns in species abundance and distributions. *Nat. Educ. Knowl.* **3**, 38 (2011).
7. Dullo, W. C., Flögel, S. & Rüggeberg, A. Cold-water coral growth in relation to the hydrography of the Celtic and Nordic European continental margin. *Mar. Ecol. Prog. Ser.* **371**, 165–176 (2008).
8. Davies, A. J. & Guinotte, J. M. Global habitat suitability for framework-forming cold-water corals. *PLoS one* **6**, e18483 (2011).
9. Yesson, C. et al. Global habitat suitability of cold-water octocorals. *J. Biogeogr.* **39**, 1278–1292 (2012).
10. Bernardino, A. F., Berenguer, V. & Ribeiro-Ferreira, V. P. Bathymetric and regional changes in benthic macrofaunal assemblages on the deep Eastern Brazilian margin, SW Atlantic. *Deep Sea Res. Part I Oceanogr. Res. Pap.* **111**, 110–120 (2016).
11. Cavalcanti, G. H. et al. Ecosistemas de corais de águas profundas da Bacia de Campos. In *Comunidades Demersais e Bioconstrutores: caracterização ambiental regional da Bacia de Campos, Atlântico Sudoeste* (eds. Curbelo-Fernandez, M. P. & Braga, A. C.). 43–85 (Elsevier, 2017).
12. Sumida, P. Y. G., De Leo, F. C. & Bernardino, A. F. An Introduction to the Brazilian Deep-Sea Biodiversity. In *Brazilian deep-sea biodiversity* (eds. Sumida, P. Y. G., Bernardino, A. F. & De Leo, F. C.) 1–5 (Springer, 2020).
13. Freiwald, A., Fossa, J. H., Grehan, A., Koslow, T. & Roberts, M. J. In *Cold-water Coral Reefs: out of sight-no longer out of mind* (eds. Hain, S. & Corcoran, E.) 1–86 (UNEP-WCMC, 2004).
14. Silveira, I. C. A., Napolitano, D. C., & Farias, I. U. Water Masses and Oceanic Circulation of the Brazilian Continental Margin and Adjacent Abyssal Plain. In *Brazilian deep-sea biodiversity* (eds. Sumida, P. Y. G., Bernardino, A. F. & De Leo, F. C.) 7–36 (Springer, 2020).
15. Barbosa, R. V., Davies, A. J. & Sumida, P. Y. G. Habitat suitability and environmental niche comparison of cold-water coral species along the Brazilian continental margin. *Deep Sea Res. Part I Oceanogr. Res. Pap.* **155**, 103147 (2020).
16. Gómez, C. E. et al. Natural variability in seawater temperature compromises the metabolic performance of a reef-forming cold-water coral with implications for vulnerability to ongoing global change. *Coral Reefs* **41**, 1–13 (2022).
17. Dorey, N., Gjelsvik, Ø., Kutti, T., & Büscher, J. V. Broad thermal tolerance in the cold-water coral *Lophelia pertusa* from Arctic and boreal reefs. *Front. Physiol.* **10**, 1–12 (2020).
18. Brooke, S., Ross, S. W., Bane, J. M., Seim, H. E. & Young, C. M. Temperature tolerance of the deep-sea coral *Lophelia pertusa* from the southeastern United States. *Deep Sea Res. II: Top. Stud. Oceanogr.* **92**, 240–248 (2013).
19. Kurman, M. D., Gomez, C. E., Georgian, S. E., Lunden, J. J. & Cordes, E. E. Intra-specific variation reveals potential for adaptation to ocean acidification in a cold-water coral from the Gulf of Mexico. *Front. Mar. Sci.* **4**, 111 (2017).
20. White, M., Mohn, C., de Stigter, H. & Mottram, G. Deep-water coral development as a function of hydrodynamics and surface productivity around the submarine banks of the Rockall Trough, NE Atlantic. In *Cold-water Corals and Ecosystems* (eds. Freiwald, A. & Roberts, J. M.) 503–514 (Springer, 2005).
21. Biló, T. C., da Silveira, I. C. A., Belo, W. C., de Castro, B. M. & Piola, A. R. Methods for estimating the velocities of the Brazil current in the pre-salt reservoir area off southeast Brazil (23° S–26° S). *Ocean Dyn.* **64**, 1431–1446 (2014).
22. Wienberg, C. et al. The giant Mauritanian cold-water coral mound province: oxygen control on coral mound formation. *Quat. Sci. Rev.* **185**, 135–152 (2018).
23. Sanna, G. & Freiwald, A. Deciphering the composite morphological diversity of *Lophelia pertusa*, a cosmopolitan deep-water ecosystem engineer. *Ecosphere* **12**, e03802 (2021).
24. Arantes, R. C. M. et al. Depth and water mass zonation and species associations of cold-water octocoral and stony coral communities in the southwestern Atlantic. *Mar. Ecol. Prog. Ser.* **397**, 71–79 (2009).
25. Cordeiro, R. T. S. et al. First assessment on Southwestern Atlantic equatorial deep-sea coral communities. *Deep Sea Res. I: Oceanogr. Res. Pap.* **163**, 103344 (2020).
26. Pires, D. O. The azooxanthellate coral fauna of Brazil. In *Conservation and adaptive management of seamount and deep-sea coral ecosystems* (eds. George, R. Y. & Cairns, S. D.) 265–272 (Rosenstiel School of Marine and Atmospheric Science, 2007).
27. Raddatz, J. et al. *Solenosmilia variabilis* bearing cold-water coral mounds off Brazil. *Coral Reefs* **39**, 69–83 (2020).
28. Cairns, S. D. Studies on western atlantic octocorallia (Gorgonacea: Primnoidae). Part 8: new records of primnoidae from the new England and corner rise seamounts. *Proc. Biol. Soc. Wash.* **120**, 243–263 (2007).
29. Mazzini, P. L. F. & Barth, J. A. A comparison of mechanisms generating vertical transport in the Brazilian coastal upwelling regions. *J. Geophys. Res. Oceans* **118**, 5977–5993 (2013).
30. Calado, L., Silveira, I. C. A., Gangopadhyay, A. & De Castro, B. M. Eddy-induced upwelling off Cape São Tomé (22 S, Brazil). *Cont. Shelf Res.* **30**, 1181–1188 (2010).
31. Lehmann, A. & Myrberg, K. Upwelling in the Baltic Sea—a review. *J. Mar. Sys.* **74**, S3–S12 (2008).
32. Coelho-souza, S. A. et al. Biophysical interactions in the Cabo Frio upwelling system, Southeastern Brazil. *Braz. J. Oceanogr.* **60**, 353–365 (2012).
33. Maly et al. The Alpha Crucis Carbonate Ridge (ACCR): discovery of a giant ring-shaped carbonate complex on the SW atlantic margin. *Sci. Rep.* **9**, 1–10 (2019).
34. Sumida, P. Y. G., Yoshinaga, M. Y., Madureira, L. A. S. P. & Hovland, M. Seabed pockmarks associated with deepwater corals off SE Brazilian continental slope, Santos Basin. *Mar. Geol.* **207**, 159–167 (2004).
35. Schattner, U., Lazar, M., Souza, L. A. P., Ten Brink, U. & Mahiques, M. M. D. Pockmark asymmetry and seafloor currents in the Santos Basin offshore Brazil. *Geo-Mar. Lett.* **36**, 457–464 (2016).
36. Zeppilli, D., Mea, M., Corinaldesi, C. & Danovaro, R. Mud volcanoes in the mediterranean sea are hot spots of exclusive meiobenthic species. *Prog. Oceanogr.* **91**, 260–272 (2011).
37. Carrerette, O. et al. Macrobenthic assemblages across deep-sea pockmarks and carbonate mounds at Santos Basin, SW Atlantic. *Ocean Coast. Res.* **70**, 1–22 (2022).
38. Kitahara, M. V. Novas ocorrências de corais azooxantelados (Anthozoa, Scleractinia) na plataforma e talude continental do sul do Brasil (25–34° S). *Biotemas* **19**, 55–63 (2006).
39. Kitahara, M. V. Species richness and distribution of azooxanthellate scleractinia in Brazil. *Bull. Mar. Sci.* **81**, 497–518 (2007).
40. Cavalcanti, G. H. et al. Ambientes de corais de águas profundas da Bacia de Santos, Brasil (Atlântico Sudoeste). COLACMAR (2013).
41. Pires, D. O., Silva, J. C. & Bastos, N. D. Reproduction of deep-sea reef-building corals from the southwestern atlantic. *Deep Sea Res. II: Top. Stud. Oceanogr.* **99**, 51–63 (2014).
42. McLean, D. L. et al. Enhancing the scientific value of industry remotely operated vehicles (ROVs) in our oceans. *Front. Mar. Sci.* **7**, 220 (2020).
43. Hovland, M., Vasshus, S., Indreide, A., Austdal, L. & Nilsen, Ø. Mapping and imaging deep-sea coral reefs off Norway, 1982–2000. *Hydrobiologia* **471**, 13–17 (2002).
44. Gates, A. R. et al. Deep-sea observations at hydrocarbon drilling locations: contributions from the SERPENT project after 120 field visits. *Deep Sea Res. Part II Top. Stud. Oceanogr.* **137**, 463–479 (2017).
45. Loya, Y., Puglise, K. A. & Bridge, T. C. In *Mesophotic Coral Ecosystems* (eds. Loya, Y., Puglise, K. A. & Bridge, T. C. L.) 1–1003 (Springer, 2019).
46. Quattrini, A. M., Gómez, C. E. & Cordes, E. E. Environmental filtering and neutral processes shape octocoral community assembly in the deep sea. *Oecologia* **183**, 221–236 (2017).
47. Mohriak, W. U. Bacias sedimentares da margem continental Brasileira. *Geologia, tectônica e recursos minerais do Brasil* **3**, 87–165 (2003).
48. Mahiques, M. M. et al. Hydrodynamically driven patterns of recent sedimentation in the shelf and upper slope off Southeast Brazil. *Cont. Shelf Res.* **24**, 1685–1697 (2004).
49. Figueiredo, A. G. Jr, Carneiro, J. C. & Santos Filho, J. R. D. Santos Basin continental shelf morphology, sedimentology, and slope sediment distribution. *Ocean Coast. Res.* **71**, e23007 (2023).
50. Piola, A. R. et al. Physical oceanography of the SW Atlantic Shelf: a review. Plankton ecology of the Southwestern Atlantic, 37–56 (2018).
51. Valla, D., Piola, A. R., Meinen, C. S. & Campos, E. Strong mixing and recirculation in the northwestern Argentine Basin. *J. Geophys. Res. Oceans* **123**, 4624–4648 (2018).
52. Jackett, D. R. & McDougall, T. J. A neutral density variable for the world's oceans. *J. Phys. Oceanogr.* **27**, 237–263 (1997).
53. Howell, K. L., Davies, J. S. & Narayanaswamy, B. E. Identifying deep-sea megafaunal epibenthic assemblages for use in habitat mapping and marine protected area network design. *J. Mar. Biol. Assoc. U.K.* **90**, 33–68 (2010).
54. Zibrowius, H. Les Scléractiniales de la Méditerranée et de l'Atlantique nord-oriental. *Mémoires de l'Institut océanographique*. 226 pp (1980).
55. Cairns, S. D. A revision of the ahermatypic Scleractinia of the Galápagos and Cocos islands. *Smithson. Contrib. Zool.* **504**, 1–30 (1991).
56. Zibrowius, H. & Cairns, S. D. *Revision of the northeast Atlantic and Mediterranean Stylasteridae (Cnidaria: Hydrozoa)*. Mémoires du Muséum national d'Histoire naturelle, Paris, Séries A Zoologie. 135pp (1992).

57. Opresko, D. M. Revision of the Antipatharia (Cnidaria: Anthozoa). Part V. Establishment of a new family, Stylopathidae. *Zool. Meded.* **80**, 109–138 (2006).
58. Smith, E. P. & van Belle, G. Nonparametric estimation of species richness. *Biometrics* **40**, 119–129 (1984).
59. Colwell, R. K., Mao, C. X. & Chang, J. Interpolating, extrapolating and comparing incidence-based species accumulation curves. *Ecology* **85**, 2717–2727 (2004).
60. Colwell, R. K. EstimateS. Statistical estimation of species richness and shared species from samples. Version 910. User's Guide and applications. (2013).
61. Anderson, M. J. A new method for non-parametric multivariate analysis of variance. *Austral Ecol.* **26**, 32–46 (2001).
62. Martinez Arbizu, P. PairwiseAdonis: Pairwise Multilevel Comparison Using Adonis. R package. <https://github.com/pmartinezarbizu/pairwiseAdonis>. (2022).
63. Kohonen, T. Self-organized formation of topologically correct feature maps. *Biol. Cybern.* **43**, 59–69 (1982).
64. Kohonen, T. In *Self-organizing maps* (ed. Kohonen, T.). 1–502 (Springer, 2001). <https://doi.org/10.1007/978-3-642-56927-2>.
65. Vieira, D. C. & Fonseca, G. iMESc: an interactive machine learning app for environmental science (2022).
66. Fraser, S. J., & Dickson, B. L. A new method for data integration and integrated data interpretation: self-organising maps. In *Proceedings of exploration* (ed. Milkereit, B.) **7**, 907–910 (2007).
67. Melsens, W. J., Smits, J. R. M., Buydens, L. M. C. & Kateman, G. Using artificial neural networks for solving chemical problems: part II. Kohonen self-organising feature maps and Hopfield networks. *Chemometr. Intell. Lab. Syst.* **23**, 267–291 (1994).
68. Park, Y. S., Céréghino, R., Compin, A. & Lek, S. Applications of artificial neural networks for patterning and predicting aquatic insect species richness in running waters. *Ecol. Model.* **160**, 265–280 (2003).
69. Yuan, C. & Yang, H. Research on K-value selection method of K-means clustering algorithm. *J.* **2**, 226–235 (2019).
70. Legendre, P. & Legendre, L. *Numerical ecology*, 3rd English edition. Amsterdam, The Netherlands: Elsevier Science BV (2012).
71. Oksanen et al. vegan: Community ecology package. R package version 2.5-4 (2019).
72. Hastie, T. & Tibshirani, R. Generalized additive models (with Discussion). *Stat. Sci.* **1**, 336–337 (1986).

Acknowledgements

We would like to express our gratitude to Petrobras for their financial support and for the complementary data for this study through the PCR-BS Project (Santos Basin Environmental Characterization). We would also like to make a special acknowledgement for the support from the Universidade de São Paulo. N.F.C. was supported by grant #2018/13141-5 from the Fundação de Amparo à Pesquisa do Estado de São Paulo (FAPESP) and was financed in part by grant #141788/2018-6 from the Conselho Nacional de Desenvolvimento Científico e Tecnológico (CNPq). We would also like to extend our thanks to cnidarian taxonomists Dr. Marcelo Kitahara, Dr. Andrea Quattrini,

Dr. Jeremy Horowitz, and Dr. Steve Auscavitch for their assistance with deep-sea coral taxonomic resolution IDs.

Author contributions

N.F.C. and P.Y.G.S. designed the study. R.C.M.A. and G.H.C. performed habitat verification through pilot studies, site selection, and participated in the ROV data collection. N.F.C. processed image analysis, led writing of the manuscript, analyzed main results and produced most figures. E.E.C. and R.C.M.A. performed the validation of most species. C.M.H. worked on the underlying data that generated the study map. D.K.S. and M.D. organized and selected information from the CTD data collection, and provided the analysis of water masses structure. L.G.W. performed the English proofreading. L.G.W., R.C.M.A., D.M.C., G.H.C., A.Z.G., C.M.H., A.P.C.F., P.D.N., D.K.S., M.D., E.E.C. and P.Y.G.S. contributed to editing and discussion of the manuscript.

Competing interests

The authors declare no competing interests.

Additional information

Supplementary information The online version contains supplementary material available at <https://doi.org/10.1038/s43247-023-00924-0>.

Correspondence and requests for materials should be addressed to Nayara F. Carvalho or Paulo Y. G. Sumida.

Peer review information *Communications Earth & Environment* thanks Thomas Hourigan and the other, anonymous, reviewer(s) for their contribution to the peer review of this work. Primary Handling Editors: Annie Bourbonnais, Joe Aslin and Clare Davis.

Reprints and permission information is available at <http://www.nature.com/reprints>

Publisher's note Springer Nature remains neutral with regard to jurisdictional claims in published maps and institutional affiliations.



Open Access This article is licensed under a Creative Commons Attribution 4.0 International License, which permits use, sharing, adaptation, distribution and reproduction in any medium or format, as long as you give appropriate credit to the original author(s) and the source, provide a link to the Creative Commons licence, and indicate if changes were made. The images or other third party material in this article are included in the article's Creative Commons licence, unless indicated otherwise in a credit line to the material. If material is not included in the article's Creative Commons licence and your intended use is not permitted by statutory regulation or exceeds the permitted use, you will need to obtain permission directly from the copyright holder. To view a copy of this licence, visit <http://creativecommons.org/licenses/by/4.0/>.

© The Author(s) 2023